MAVEN Observations of H- Ions in the Martian Atmosphere

Nicholas Jones[1], Jasper S. Halekas[1], Zachary Girazian[2], David L. Mitchell[3], and Christian Mazelle[4]

[1]University of Iowa
[2]The University of Iowa
[3]University of California, Berkeley
[4]Institut de Recherche en Astrophysique et Planetologie

November 23, 2022

Abstract

At Mars, charge exchange between solar wind protons and neutral exospheric hydrogen produces energetic neutral atoms (ENAs) that can penetrate into the collisional atmosphere, where they can be converted through collisions into H^+ and H^-. The Mars Atmosphere and Volatile EvolutioN (MAVEN) mission observed a population of negatively charged particles at low altitudes, whose energies, angular distribution, and dependence on the upstream solar wind were consistent with H^-originating in the solar wind. The highest fluxes of H^- were observed near perihelion and the southern summer solstice. We calculated an average ratio of ˜4% between H^- density and H^+ density, implying a slightly smaller relative abundance than reported previously (˜10%). We found that the fraction of H ENAs converted to H^- increases with the solar wind energy, in agreement with laboratory measurements of the H–CO_2 electron capture cross section.

MAVEN Observations of H^- Ions in the Martian Atmosphere

Enter authors here: N. Jones[1], J. Halekas[1], Z. Girazian[1], D. Mitchell[2], and C. Mazelle[3]

[1]Department of Physics and Astronomy, University of Iowa, Iowa City, Iowa, USA

[2]Space Sciences Laboratory, University of California, Berkeley, California, USA

[3]L'Institut de Recherche en Astrophysique et Planétologie, Toulouse, France

Corresponding author: Nicholas Jones (nicholas-a-jones@uiowa.edu)

Key Points:

- We observed H^- in the Martian atmosphere at low altitudes with solar wind energies
- Fluxes of H^- varied seasonally, with a maximum near perihelion and the southern summer solstice
- We found a ratio of about four percent between H^- density and H^+ density, lower than previously reported ratios

Abstract

At Mars, charge exchange between solar wind protons and neutral exospheric hydrogen produces energetic neutral atoms (ENAs) that can penetrate into the collisional atmosphere, where they can be converted through collisions into H^+ and $H^–$. The Mars Atmosphere and Volatile EvolutioN (MAVEN) mission observed a population of negatively charged particles at low altitudes, whose energies, angular distribution, and dependence on the upstream solar wind were consistent with $H^–$ originating in the solar wind. The highest fluxes of $H^–$ were observed near perihelion and the southern summer solstice. We calculated an average ratio of ~4% between $H^–$ density and H^+ density, implying a slightly smaller relative abundance than reported previously (~10%). We found that the fraction of H ENAs converted to $H^–$ increases with the solar wind energy, in agreement with laboratory measurements of the H–CO_2 electron capture cross section.

Plain Language Summary

At Mars, interactions between solar wind protons and neutral hydrogen in the outer atmosphere produces energetic neutral atoms (ENAs) that travel into the inner atmosphere, where collisions with atmospheric gas can produce H^+ ions and $H^–$ ions. The Mars Atmosphere and Volatile EvolutioN (MAVEN) missions observed $H^–$ ions in the inner atmosphere, with energies and velocities that matched the solar wind. The highest fluxes of $H^–$ ions were seen when Mars was closest to the Sun, during the southern summer. We found that the relative amount of $H^–$ ions to H^+ ions was smaller than previous studies had found. We also found that the amount of $H^–$ ions produced depended on the solar wind energy, a result that agrees with laboratory experiments.

1 Introduction

In addition to a collisional atmosphere, Mars has a neutral hydrogen exosphere that extends to altitudes of several Martian radii (Anderson, 1974; Chaufray et al., 2008). A portion of the exosphere extends to altitudes upstream of the Martian bow shock, where incoming solar wind protons can undergo charge exchange with neutral exospheric hydrogen to produce energetic neutral atoms (ENAs) moving towards Mars with the original solar wind velocity (Kallio et al., 1997; Holmström et al., 2002; Gunell et al., 2006). Uninhibited by electromagnetic fields, the ENAs can pass through the bow shock and into the collisional atmosphere, where collisions with atmospheric gases can cause energy deposition (Kallio & Barabash, 2001), proton aurora (Ritter et al., 2018; Deighan et al., 2018), and angular spreading and backscatter (Kallio & Barabash, 2001; Shematovich et al., 2011; Halekas et al., 2015; Bisikalo et al., 2018; Girazian & Halekas, 2021). The ENAs can also undergo electron stripping or electron attachment in collisions with atmospheric neutrals, producing both positive (Kallio & Barabash, 2001; Halekas et al., 2015) and negative (Halekas et al., 2015) hydrogen ions.

Hydrogen ENAs have been observed at Mars by Mars Express (MEX) (Gunell et al., 2006; Futaana et al., 2006; Brinkfeldt et al., 2006; Mura et al., 2008; Wang et al., 2013). However, MEX periapsis altitudes of ~270 km lie above altitudes of peak ENA energy deposition. Mars Atmosphere and Volatile EvolutioN (MAVEN)'s lower altitude periapsis of ~150 km provides an opportunity to observe the charged products of ENA collisions at altitudes of peak energy deposition. Indeed, Halekas et al. (2015) observed a ubiquitous flux of H^+ ions and an occasional flux of $H^–$ ions at low altitudes, with energies corresponding to the upstream solar wind. In this manuscript, we more closely examine the $H^–$ ions detected by MAVEN at low altitudes.

Similar effects occur at comet 67P/Churyumov–Gerasimenko, where H^- ions have been detected by the Ion and Electron Sensor aboard Rosetta (Burch et al., 2015). Here, H^- ions were observed with fluxes of ~10% of the proton fluxes and energies of ~90% of the proton energies. Burch et al. (2015) concluded that the observed fluxes and energies were consistent with H^- ion production via double charge exchange between solar wind protons and molecules in the coma. The study at comet 67P provides a valuable comparison for our own study of H^- ions at Mars.

2 Data

We used data from MAVEN's Solar Wind Electron Analyzer (SWEA) (Mitchell et al., 2016), an electrostatic analyzer that measures negatively charged particles between 3 eV and 4.6 keV. SWEA has an energy resolution of $\Delta E/E = 17\%$, a measurement cadence of 2 seconds, and a field of view of 360° × 120° (azimuth × elevation) with an angular resolution of 22.5° × 20° (azimuth × elevation). Although designed to measure electrons in the Mars environment, SWEA is capable of detecting any particle with a negative charge and an energy per charge in the detectable range, including the H^- ions of interest in our study.

Our analysis included 3150 MAVEN orbits occurring between 07 October 2014 and 22 February 2020. We required that MAVEN be orbiting on the dayside of Mars during spacecraft periapsis, such that the area of observation was directly downstream of the solar wind. This allowed us to compare SWEA's measurements with the upstream solar wind, which was measured on the same orbits by MAVEN's Solar Wind Ion Analyzer (SWIA) (Halekas et al., 2015). We filtered out orbits where the upstream solar wind energy was below 600 eV so that H^- ions originating in the solar wind would be separated from the significant fluxes of photoelectrons, including Auger electrons at ~500 eV (Mitchell et al., 2000).

Figure 1 shows an example of SWEA data from a single periapsis pass on 08 March 2015. The top and middle panels are angle–integrated spectrograms covering 30 minutes, centered on the time of periapsis, and the bottom panel is a time–series plot of the spacecraft altitude. The top panel is averaged over surface–looking directions and depicts fluxes and energies of particles with sunward velocities, while the middle panel is averaged over space–looking directions and depicts fluxes and energies of particles with anti–sunward velocities. At low energies, MAVEN observed significant fluxes of electrons in both the sunward and anti–sunward velocity directions. At altitudes below ~200 km, MAVEN observed a low–flux signal exclusively in the anti–sunward velocity direction, with energies corresponding to the solar wind energies (~3 keV at this time). The energy and angular distribution of this signal are consistent with particles originating in the solar wind, while the low altitude and negative charge are consistent with H^- ions produced in collisions between penetrating ENAs and gas in the collisional atmosphere.

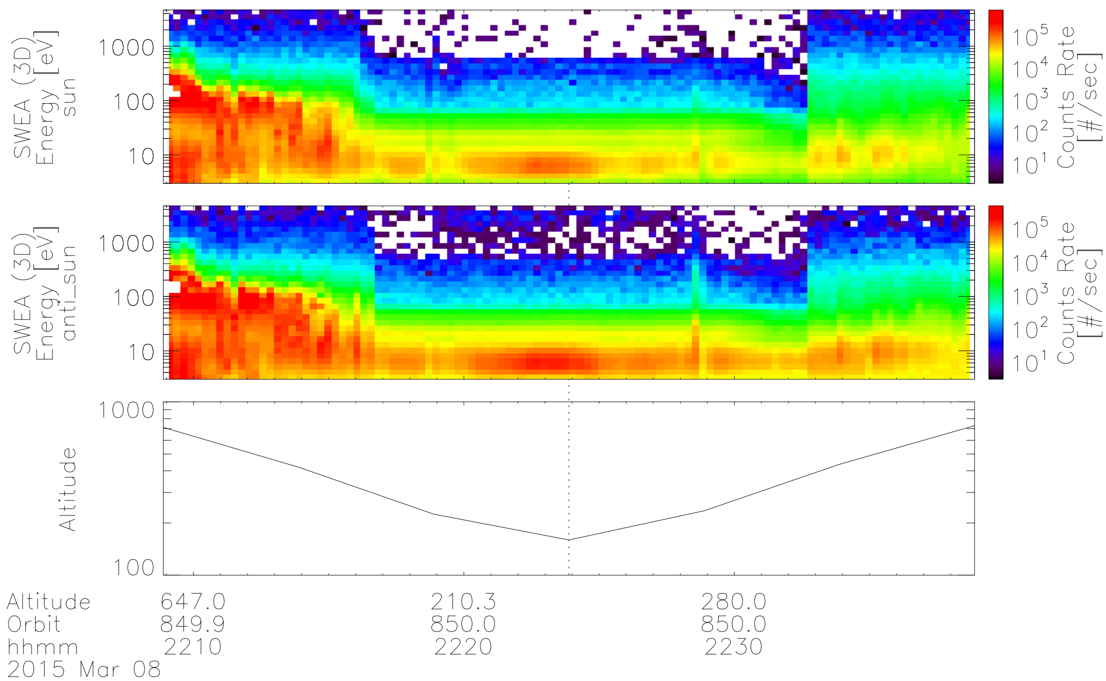

Figure 1. Angle–integrated time–series plots of SWEA 3D survey data for sunward (top) and anti–sunward (middle) particle velocities, covering 30 minutes centered on the time of periapsis for a MAVEN orbit on 08 March 2015. The spacecraft altitude (bottom) is also shown. SWEA observed high fluxes of photoelectrons at low energies in both velocity directions. At altitudes below ~200 km, there is low–flux signal at high energies seen exclusively in the anti–sunward velocity direction, which we interpret as H^- ions originating in the solar wind.

It is worth noting that the data shown in figure 1 was taken during a MAVEN orbit that followed a high–speed interplanetary coronal mass ejection (CME). The CME dramatically increased the number of charged particles incident on the Martian exosphere, leading to a significant increase in the penetrating ENA flux and subsequently a significant increase in the H^- flux observed at low altitudes. During times with more typical solar wind conditions, both the energy and flux of the low–altitude H^- population were lower than seen in figure 1 (and sometimes were not detectable at all). We chose to use the above orbit as an example because of the clarity of the H^- signal and the clear difference in flux between the sunward and anti–sunward velocity directions.

3 Flux–Energy Spectra

For every orbit in our analysis, we averaged the flux measured by SWEA during times when the spacecraft altitude was below 300 km, for both the sunward and anti–sunward velocity directions. Plotting the averaged fluxes against the detector energies, we created time–averaged and angle–averaged flux–energy spectra. Figure 2 shows both the sunward (dashed) and anti–sunward (solid) flux–energy spectra for a MAVEN orbit on 08 March 2015 (the same orbit used in figure 1). Visible in both spectra are peaks around ~20 eV from photoionization of CO_2 and O (Frahm et al., 2006), and ~500 eV from Auger electrons produced by *K* shell ionization of atmospheric gases (Mitchell et al., 2000; Sakai et al., 2015). Above ~800 eV the two spectra diverge, with a peak in the anti–sunward spectrum around ~3 keV corresponding to H^- ions produced by solar wind ENA reconversion.

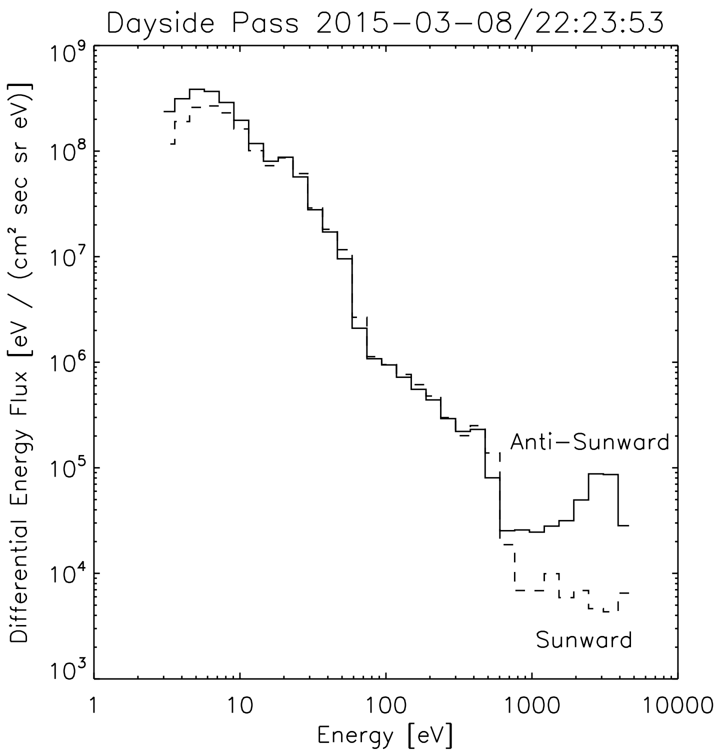

Figure 2. Time–averaged and angle–averaged flux–energy spectra for sunward (dashed) and anti–sunward (solid) particle velocities. The fluxes were averaged over times where the spacecraft altitude was below 300 km, during a MAVEN periapsis pass on 08 March 2015. At energies above ~800 eV, the two spectra diverge revealing a population of negatively charged particles with anti–sunward velocities, with a peak near ~3 keV.

We do not expect to see any significant flux of negatively charged particles at high energies and low altitudes in the sunward velocity direction. Although some H^- ions may experience enough collisions to be backscattered into the sunward velocity direction, the expected energy loss from such collisions would cause the backscatter fluxes to be obscured by the high fluxes of electrons. Combined with the low flux of H^- ions to begin with, it is unlikely that we would be able to detect any backscattered H^-. We therefore considered the high–energy flux seen in the sunward velocity direction to be entirely background, resulting from natural radioactivity in the microchannel plate detectors and/or penetrating galactic cosmic rays. For each orbit in our analysis, we calculated the background flux by averaging the flux measured in the four highest detector energy bins for the sunward velocity direction. For orbits where data was missing at high energies in the sunward velocity direction, we used the average background flux from all other orbits. We created corrected flux–energy spectra by subtracting the background value from the flux measured at each detector energy.

The monodirectional velocities of the H^- ions that SWEA observed at energies above ~800 eV are indicative of particles with origins in the solar wind. Therefore, we expect the fluxes and energies of these H^- ions to depend on the conditions of the upstream solar wind. SWIA measured the solar wind with both direct observations of upstream solar wind protons and observations of penetrating protons in the atmosphere converted to an estimate of the upstream solar wind. We grouped MAVEN orbits based on the upstream solar wind energy measured by SWIA during each orbit and averaged the SWEA background–corrected anti–sunward flux–energy spectra for each solar wind energy group. Figure 3 shows four flux–energy spectra corresponding to four solar wind energy ranges, which together contain all 3150 MAVEN orbits used in our study. Below detector energies of ~800 eV the spectra are dominated by fluxes of photoelectrons, which are independent of the solar wind. The familiar H^- signal shows up at solar wind energies greater than 1 keV, suggesting that solar wind protons must have sufficiently high energy to produce H^- ions that are detectable above the electron fluxes. As the upstream solar wind energy increases, both the peak flux and the peak energy of the H^- ions increase, as expected.

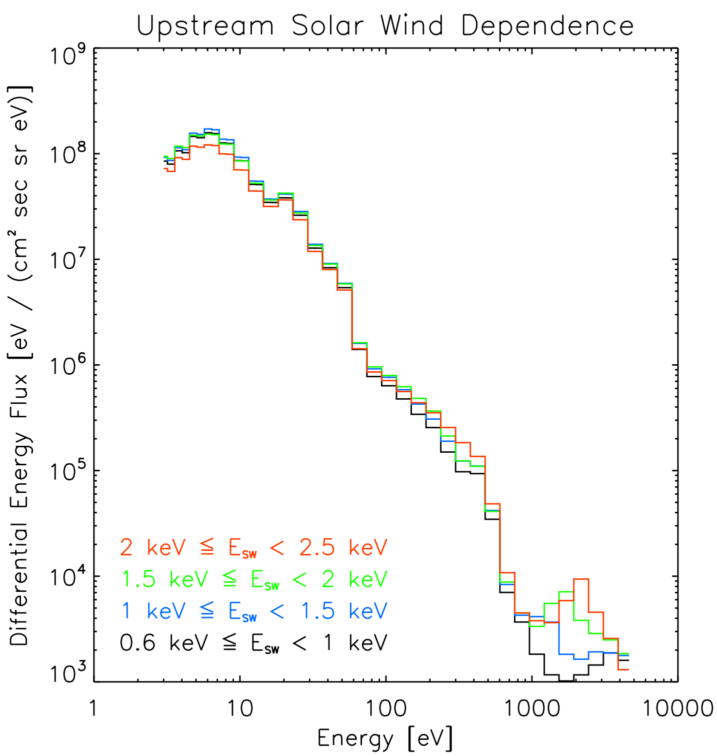

Figure 3. Four flux–energy spectra, averaged over solar wind energies. The spectra were calculated using the background–corrected anti–sunward spectra of the individual orbits. H^- ions

were detected above ~800 eV for solar wind energies above 1 keV. At higher solar wind energies, both the peak flux and the peak energy of the H^- ions increase.

4 Seasonal Variation

Over the course of the Martian year, the neutral hydrogen column density upstream of the bow shock varies significantly, with the highest densities occurring near perihelion and the southern summer solstice (Clarke et al., 2014; Halekas, 2017). The flux of hydrogen ENAs produced by charge exchange is proportional to the neutral density, as discussed by Burch et al. (2015). Because the flux of H^- ions should depend on the flux of ENAs, we expect to observe increased fluxes of H^- ions during times of increased neutral density. We binned MAVEN orbits by Martian solar longitude and calculated the average flux of H^- for each bin, identifying the H^- flux for each orbit as the peak flux measured by SWEA above 1 keV. Figure 4 shows the average flux of H^- at each solar longitude bin, with each bin spanning 60° in L_S. At high L_S, the H^- flux is increased by a factor of ~2, with the highest average flux seen between L_S = 240° and L_S = 300°. This range contains perihelion and the southern summer solstice, where the highest fluxes are expected. The seasonal increase in H^- flux coincides with the seasonal increase in neutral density, and the factor ~2 increase is reasonable given the change in exospheric neutral column density calculated by Halekas (2017).

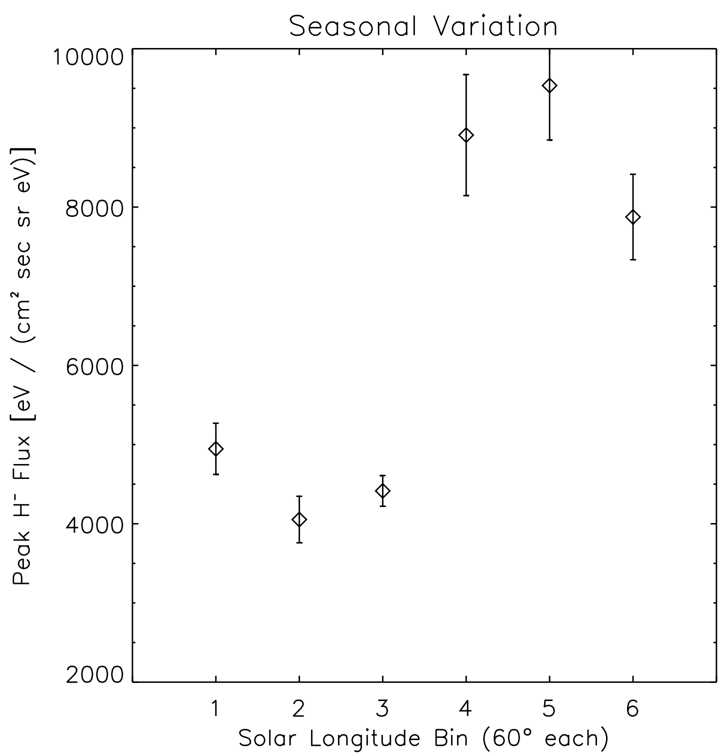

Figure 4. Average flux of H^- ions for 6 Martian solar longitude bins. Each bin spans 60° of L_S, or two Martian months. Average fluxes were calculated using the peak flux measured by SWEA

above 1 keV. The flux of H^- ions increased by a factor of ~2 at high L_S, with a maximum occurring at $240° \le L_S \le 300°$. Error bars correspond to the standard error of the mean.

5 Charge State Density Ratios

Hydrogen ENAs streaming through the collisional atmosphere experience electron stripping and electron attachment in collisions with atmospheric gas, producing H^+ ions and H^- ions, respectively. The relative abundance of each charge state was measured at comet 67P (Burch et al., 2015), where the fluxes of H^- were ~10% of the fluxes of H^+. Early observations at Mars by MAVEN (Halekas et al., 2015) also found H^- fluxes that were ~10% that of H^+ fluxes. We examined the relative amounts of each charge state by comparing the densities of H^- measured by SWEA to the densities of H^+ measured by SWIA. For 418 orbits, where low–altitude SWEA and SWIA data were both available, we calculated the H^- density moment n_{H-} using a weighted sum:

$$\boldsymbol{n_{H-} = (7.225 \times 10^{-7}) \cdot d\Omega \cdot \sum dE \cdot E^{-1.5} \cdot F_{H-}}$$

where $d\Omega = \pi/\sqrt{2}$ is the solid angle covered by the measurement, dE is the width of each energy bin, E is the particle (and bin) energies, F_{H-} is the background–corrected differential energy fluxes, and the sum is over energy bins above 800 eV. The constant fixes the units, assuming the measured ions have the mass of hydrogen. The average H^- density was 1.416×10^{-4} particles/cm^3, and the average H^-/H^+ density ratio was ~4%. This result agrees reasonably well with the ratios reported by Burch et al. (2015) and Halekas et al. (2015).

While collisions between ENAs and atmospheric gases produce H^- ions and H^+ ions, backreactions also occur, converting H^- and H^+ back to a neutral state. The amounts of H^- and H^+ present at a given time are ultimately determined by the relevant cross sections (electron capture for H^-, electron loss for H^+) and backreactions (photodetachment and charge exchange for H^-, primarily charge exchange for H^+). Laboratory measurements indicate a ratio of ~10% between the electron capture and electron loss cross sections in collisions between 1 keV H and CO_2 (Lindsay et al., 2005). If the backreactions for H^- and H^+ occurred at similar rates, we would expect the ratio between H^- density and H^+ density to also be ~10%. The lower ratio of ~4% that we observed suggests that backreactions more quickly convert H^- to H than charge exchange converts H^+ to H.

Ion production in the collisional atmosphere is dominated by collisions between neutral hydrogen and carbon dioxide (Kallio & Barabash, 2001). Laboratory experiments performed by Lindsay et al. (2005) measured the cross sections for electron loss and electron capture in collisions between H and CO_2 and found that both cross sections increase with the energy of the incident H atom. The analogous situation at Mars involves solar wind hydrogen ENAs incident upon atmospheric CO_2. We used the ratio between H^- density and solar wind H (H_{SW}) density as a measure of the electron capture cross section, and the upstream solar wind energy as a measure of the incident H energy. The density and energy of the upstream solar wind were measured by SWIA. Figure 5 shows the H^-/H_{SW} density ratio as a function of the upstream solar wind energy. We observed a factor of ~4 increase in the H^-/H_{SW} density ratio, a trend that compares favorably with Lindsay et al. (2005). We also examined how the ratio between H^- density and H^+ density varies with solar wind energy, as shown in figure 6. We found a flatter trend overall, which is expected since both the electron loss and electron capture cross sections increase with incident H energy.

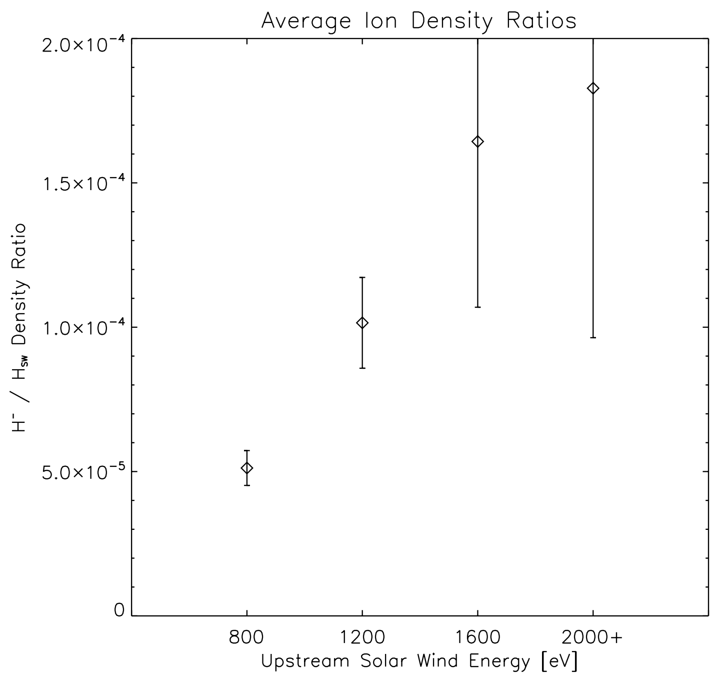

Figure 5. Average ratios of H^- density to solar wind density for four solar wind energy bins, each covering 400 eV. H^- densities were calculated with SWEA differential energy fluxes measured

above 800 eV. Solar wind densities and energies were measured by SWIA. Error bars correspond to the standard error of the mean.

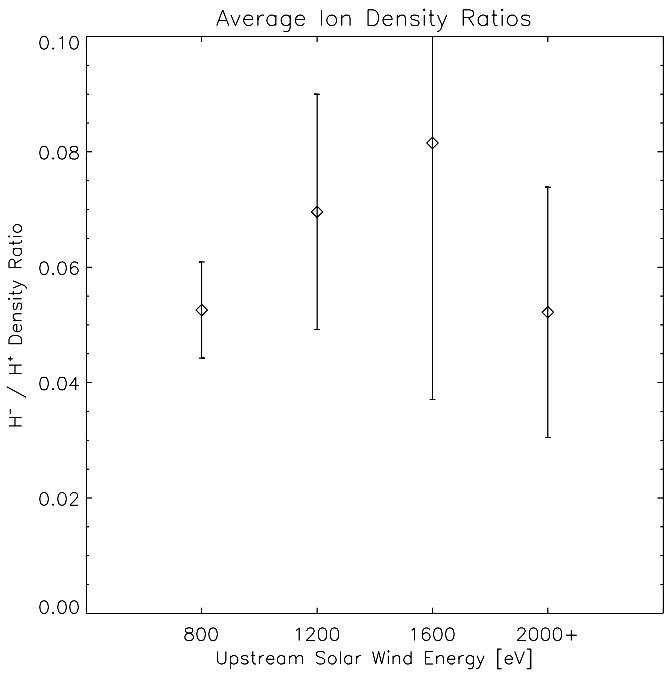

Figure 6. Average H^-/H^+ density ratios for four solar wind energy bins, each 400 eV wide. H^- densities were calculated using SWEA differential energy fluxes, and H^+ densities were calculated using SWIA penetrating proton measurements. Error bars correspond to the standard error of the mean.

6 Conclusions

MAVEN observed a population of negatively charged particles at periapsis altitudes in Mars' collisional atmosphere. The energy, angular distribution, and dependence on the upstream solar wind of these particles were consistent with H^- ions produced in collisions between H ENAs and atmospheric CO_2, with origins in the solar wind. The flux of H^- varied seasonally along with the neutral hydrogen column density upstream of the bow shock, indicating that the penetrating hydrogen ENAs likely formed through charge–changing interactions between solar wind protons and exospheric hydrogen atoms.

We calculated relative abundances of H^- ions that were similar to, although slightly smaller than, previous work at both Mars and at comet 67P/Churyumov–Gerasimenko. The smaller ratio between H^- density and H^+ density suggests that conversion of H^- back to H (through photodetachment, charge exchange) may occur more quickly than conversion of H^+ to H (primarily through charge exchange). In future work, a Monte–Carlo model could be used to track different charged species through the collisional atmosphere, taking into account the relevant reactions (collisions, charge exchange, photodetachment). Such a model could provide a useful comparison to the measured relative charge state abundances presented here. Future work could also estimate the equilibrium charged fraction, and the related detachment cross section, of H^- ions in the atmosphere using the observed H^-/H_{SW} density ratio. Such models could provide insight into the various interactions that occur between charged species in the collisional atmosphere.

Acknowledgements

We acknowledge the MAVEN contract and the Solar System Workings program through grant NNX16AO84G for support.

The datasets used in the analysis described in this manuscript are available for download on zenodo.org. DOI: 10.5281/zenodo.5090786

References

Anderson, D. E. (1974). Mariner 6, 7, and 9 Ultraviolet Spectrometer Experiment: Analysis of hydrogen Lyman alpha data. *Journal of Geophysical Research*, *79*(10), 1513–1518. https://doi.org/10.1029/JA079i010p01513

Bisikalo, D. V., Shematovich, V. I., Gérard, J.-C., & Hubert, B. (2018). Monte Carlo Simulations of the Interaction of Fast Proton and Hydrogen Atoms With the Martian Atmosphere and Comparison With In Situ Measurements. *Journal of Geophysical Research: Space Physics*, *123*(7), 5850–5861. https://doi.org/10.1029/2018JA025400

Brinkfeldt, K., Gunell, H., Brandt, P. C., Barabash, S., Frahm, R. A., Winningham, J. D., Kallio, E., Holmström, M., Futaana, Y., Ekenbäck, A., Lundin, R., Andersson, H., Yamauchi, M., Grigoriev, A., Sharber, J. R., Scherrer, J. R., Coates, A. J., Linder, D. R., Kataria, D. O., … Dierker, C. (2006). First ENA observations at Mars: Solar-wind ENAs on the nightside. *Icarus*, *182*(2), 439–447. https://doi.org/10.1016/j.icarus.2005.12.023

Burch, J. L., Cravens, T. E., Llera, K., Goldstein, R., Mokashi, P., Tzou, C.-Y., & Broiles, T. (2015). Charge exchange in cometary coma: Discovery of H^- ions in the solar wind close to comet 67P/Churyumov-Gerasimenko: NEGATIVE H IONS NEAR COMET C-G. *Geophysical Research Letters*, *42*(13), 5125–5131. https://doi.org/10.1002/2015GL064504

Chaufray, J. Y., Bertaux, J. L., Leblanc, F., & Quémerais, E. (2008). Observation of the hydrogen corona with SPICAM on Mars Express. *Icarus*, *195*(2), 598–613. https://doi.org/10.1016/j.icarus.2008.01.009

Clarke, J. T., Bertaux, J.-L., Chaufray, J.-Y., Gladstone, G. R., Quemerais, E., Wilson, J. K., & Bhattacharyya, D. (2014). A rapid decrease of the hydrogen corona of Mars: The Martian Hydrogen Corona. *Geophysical Research Letters*, *41*(22), 8013–8020. https://doi.org/10.1002/2014GL061803

Deighan, J., Jain, S. K., Chaffin, M. S., Fang, X., Halekas, J. S., Clarke, J. T., Schneider, N. M., Stewart, A. I. F., Chaufray, J.-Y., Evans, J. S., Stevens, M. H., Mayyasi, M., Stiepen, A., Crismani, M., McClintock, W. E., Holsclaw, G. M., Lo, D. Y., Montmessin, F., Lefèvre, F., & Jakosky, B. M. (2018). Discovery of a proton aurora at Mars. *Nature Astronomy*, *2*(10), 802–807. https://doi.org/10.1038/s41550-018-0538-5

Frahm, R. A., Winningham, J. D., Sharber, J. R., Scherrer, J. R., Jeffers, S. J., Coates, A. J., Linder, D. R., Kataria, D. O., Lundin, R., Barabash, S., Holmström, M., Andersson, H., Yamauchi, M., Grigoriev, A., Kallio, E., Säles, T., Riihelä, P., Schmidt, W., Koskinen, H., … Dierker, C. (2006). Carbon dioxide photoelectron energy peaks at Mars. *Icarus*, *182*(2), 371–382. https://doi.org/10.1016/j.icarus.2006.01.014

Futaana, Y., Barabash, S., Grigoriev, A., Holmström, M., Kallio, E., Brandt, P. C., Gunell, H., Brinkfeldt, K., Lundin, R., Andersson, H., Yamauchi, M., McKenna-Lawler, S., Winningham, J. D., Frahm, R. A., Sharber, J. R., Scherrer, J. R., Coates, A. J., Linder, D. R., Kataria, D. O., … Dierker, C. (2006). First ENA observations at Mars: ENA emissions from the martian upper atmosphere. *Icarus*, *182*(2), 424–430. https://doi.org/10.1016/j.icarus.2005.09.019

Girazian, Z., & Halekas, J. (2021). Precipitating Solar Wind Hydrogen at Mars: Improved Calculations of the Backscatter and Albedo With MAVEN Observations. *Journal of Geophysical Research: Planets*, *126*(2). https://doi.org/10.1029/2020JE006666

Gunell, H., Brinkfeldt, K., Holmström, M., Brandt, P. C., Barabash, S., Kallio, E., Ekenbäck, A., Futaana, Y., Lundin, R., Andersson, H., Yamauchi, M., Grigoriev, A., Winningham, J. D., Frahm, R. A., Sharber, J. R., Scherrer, J. R., Coates, A. J., Linder, D. R., Kataria, D. O., … Dierker, C. (2006). First ENA observations at Mars: Charge exchange ENAs produced in the magnetosheath. *Icarus*, *182*(2), 431–438. https://doi.org/10.1016/j.icarus.2005.10.027

Halekas, J. S. (2017). Seasonal variability of the hydrogen exosphere of Mars: Mars Hydrogen. *Journal of Geophysical Research: Planets*, *122*(5), 901–911. https://doi.org/10.1002/2017JE005306

Halekas, J. S., Lillis, R. J., Mitchell, D. L., Cravens, T. E., Mazelle, C., Connerney, J. E. P., Espley, J. R., Mahaffy, P. R., Benna, M., Jakosky, B. M., Luhmann, J. G., McFadden, J. P., Larson, D. E., Harada, Y., & Ruhunusiri, S. (2015). MAVEN observations of solar wind hydrogen deposition in the atmosphere of Mars: HYDROGEN DEPOSITION AT MARS. *Geophysical Research Letters*, *42*(21), 8901–8909. https://doi.org/10.1002/2015GL064693

Halekas, J. S., Taylor, E. R., Dalton, G., Johnson, G., Curtis, D. W., McFadden, J. P., Mitchell, D. L., Lin, R. P., & Jakosky, B. M. (2015). The Solar Wind Ion Analyzer for MAVEN. *Space Science Reviews*, *195*(1–4), 125–151. https://doi.org/10.1007/s11214-013-0029-z

Holmström, M. (2002). Energetic neutral atoms at Mars 1. Imaging of solar wind protons. *Journal of Geophysical Research*, *107*(A10), 1277. https://doi.org/10.1029/2001JA000325

Kallio, E., & Barabash, S. (2001). Atmospheric effects of precipitating energetic hydrogen atoms on the Martian atmosphere. *Journal of Geophysical Research: Space Physics*, *106*(A1), 165–177. https://doi.org/10.1029/2000JA002003

Kallio, E., Luhmann, J. G., & Barabash, S. (1997). Charge exchange near Mars: The solar wind absorption and energetic neutral atom production. *Journal of Geophysical Research: Space Physics*, *102*(A10), 22183–22197. https://doi.org/10.1029/97JA01662

Lindsay, B. G., Yu, W. S., & Stebbings, R. F. (2005). Cross sections for charge-changing processes involving kilo-electron-volt H and H^+ with CO and CO_2. *Physical Review A*, *71*(3), 032705. https://doi.org/10.1103/PhysRevA.71.032705

Mitchell, D. L., Lin, R. P., Rème, H., Crider, D. H., Cloutier, P. A., Connerney, J. E. P., Acuña, M. H., & Ness, N. F. (2000). Oxygen auger electrons observed in Mars' ionosphere. *Geophysical Research Letters*, *27*(13), 1871–1874. https://doi.org/10.1029/1999GL010754

Mitchell, D. L., Mazelle, C., Sauvaud, J.-A., Thocaven, J.-J., Rouzaud, J., Fedorov, A., Rouger, P., Toublanc, D., Taylor, E., Gordon, D., Robinson, M., Heavner, S., Turin, P., Diaz-Aguado, M., Curtis, D. W., Lin, R. P., & Jakosky, B. M. (2016). The MAVEN Solar Wind Electron Analyzer. *Space Science Reviews*, *200*(1–4), 495–528. https://doi.org/10.1007/s11214-015-0232-1

Mura, A., Orsini, S., Milillo, A., Kallio, E., Galli, A., Barabash, S., Wurz, P., Grigoriev, A., Futaana, Y., Andersson, H., Lundin, R., Yamauchi, M., Fraenz, M., Krupp, N., Woch, J., Asamura, K., Coates, A. J., Curtis, C. C., Hsieh, K. C., … Sharber, J. R. (2008). ENA detection in the dayside of Mars: ASPERA-3 NPD statistical study. *Planetary and Space Science*, *56*(6), 840–845. https://doi.org/10.1016/j.pss.2007.12.013

Ritter, B., Gérard, J. -C., Hubert, B., Rodriguez, L., & Montmessin, F. (2018). Observations of the Proton Aurora on Mars With SPICAM on Board Mars Express. *Geophysical Research Letters*, *45*(2), 612–619. https://doi.org/10.1002/2017GL076235

Sakai, S., Rahmati, A., Mitchell, D. L., Cravens, T. E., Bougher, S. W., Mazelle, C., Peterson, W. K., Eparvier, F. G., Fontenla, J. M., & Jakosky, B. M. (2015). Model insights into energetic photoelectrons measured at Mars by MAVEN: PHOTOELECTRONS AT MARS. *Geophysical Research Letters*, *42*(21), 8894–8900. https://doi.org/10.1002/2015GL065169

Shematovich, V. I., Bisikalo, D. V., Diéval, C., Barabash, S., Stenberg, G., Nilsson, H., Futaana, Y., Holmstrom, M., & Gérard, J.-C. (2011). Proton and hydrogen atom transport in the Martian upper atmosphere with an induced magnetic field: H^+/H TRANSPORT IN THE MARTIAN ATMOSPHERE. *Journal of Geophysical Research: Space Physics*, *116*(A11), n/a-n/a. https://doi.org/10.1029/2011JA017007

Wang, X.-D., Barabash, S., Futaana, Y., Grigoriev, A., & Wurz, P. (2013). Directionality and variability of energetic neutral hydrogen fluxes observed by Mars Express: ENA EMISSION AT MARS. *Journal of Geophysical Research: Space Physics*, *118*(12), 7635–7642. https://doi.org/10.1002/2013JA018876